Cu_xUTe_3: Stabilization of UTe_3 in the $ZrSe_3$ Structure Type via Copper Insertion. The Artifact of Te−Te Chains and Evidence for Distortions Due to Long Range Modulations

Rhonda Patschke,[†] Jean D. Breshears,[†] Paul Brazis,[‡] Carl R. Kannewurf,[‡] Simon J. L. Billinge,[§] and Mercouri G. Kanatzidis*,[†]

Contribution from the Department of Chemistry, Michigan State University, East Lansing, Michigan, 48824, Department of Electrical Engineering and Computer Science, Northwestern University, Evanston, Illinois, 60208, and Department of Physics and Astronomy, Michigan State University, East Lansing, Michigan 48824

Received December 13, 2000

Abstract: The ternary phase, Cu_xUTe_3 ($x = 0.25$ and 0.33), was synthesized from a 3/1/4 mixture of Cu/U/Te that was heated to 800 °C for 6 days and cooled at a rate of −4 °C h^{-1}. It adopts the monoclinic space group $P2_1/m$ with $a = 6.0838(12)$ Å, $b = 4.2140(8)$ Å, $c = 10.361(2)$ Å, $\beta = 98.83(3)°$, and $V = 262.47(9)$ Å^3 (for $x \sim 0.25$). The structure is built from UTe_3 layers of $ZrSe_3$-type that are connected in the [001] direction by Cu atoms. The Cu atoms stabilize α-UTe_3 by inserting between the layers. Cu_xUTe_3 can be prepared rationally via a soft chemistry route by reaction of Cu with α-UTe_3. The structural analysis suggests the presence of straight chains of Te atoms (∼3.0 Å apart) along the *a*-axis but this is an artifact as shown by electron diffraction studies of Cu_xUTe_3 that indicate the existence of a supercell along the *a*-axis. Pair distribution function analysis (PDF) was used to show that the Te−Te chains contain Te−Te dimers at 2.74 Å. Charge transport measurements suggest a narrow gap semiconductor but they also indicate anomalous behavior as a function of temperature with a n-type to p-type transition at ∼40 K.

Introduction

Actinide chalcogenides particularly with uranium and thorium have been investigated for many years, yet besides the rich structural and compositional diversity discovered in these systems questions remain mainly in the telluride congeners concerning their exact structures. The problem is complicated by (perhaps derives from) the well-known tendency of Te to form long-range Te···Te interactions. Understanding these interactions is important because they directly impact the physical and electronic properties of these materials. Recently, a survey of the structural chemistry of both ternary and quaternary uranium (and thorium) chalcogenides was presented.[1] Among the most notable in this class include $CsUTe_6$,[2] $Cs_8Hf_5UTe_{30.6}$,[2] $AMUQ_3$ (A = alkali or alkaline earth metal, M = 3d metal, Q = S, Se, Te),[2b,3] $CsTiUTe_5$,[2b] $Tl_{0.56}UTe_3$,[4] $K_2UP_3Se_9$,[5] $K_2ThP_3Se_9$,[6] $Cs_4Th_2P_5Se_{17}$,[6] and $Rb_4U_4P_4Se_{26}$,[7] as well as $K_6Cu_{12}U_2S_{15}$,[8] KU_2SbSe_8,[9] and RbU_2SbS_8.[9] Naturally we became interested in the copper uranium telluride system that afforded the interesting phase Cu_xUTe_3 ($x = 0.25$ and 0.33). Only two other ternary copper uranium chalcogenide phases have been reported (i.e.: $Cu_2U_3Q_7$[10] and $Cu_2U_6Q_{13}$ (Q = S, Se)[11]) which were found in the sulfide and selenide systems. Although formulated differently, Cu_xUTe_3 ($x = 0.25$ and 0.33) is isostructural to $CuTh_2Te_6$[12] and adopts the layered $ZrSe_3$ structure type. Structurally, these ternary compounds derive from the parent binary layered phases by inserting copper atoms between the layers. The occupancy of the copper site ranges from 0.25 to 0.50. In this sense, these compounds can be compared to the intercalation compounds, Li_xZrQ_3 ($0 < x \leq 3$).[13,14] The structural distortions occurring upon intercalation, such as the insertion of metal atoms between the $ZrSe_3$-type layers, are not well understood. In addition to the Li_xZrSe_3 ($0 < x \leq 3$) phases, a series of compounds with the formula ATh_2Q_6 (A = K, Rb, and Cs; Q = Se and Te)[15] has been reported where an alkali metal cation has been inserted between

[†] Department of Chemistry, Michigan State University.
[‡] Northwestern University.
[§] Department of Physics and Astronomy, Michigan State University.

(1) Narducci A. A.; Ibers, J. A. *Chem. Mater.* **2000**, *10*, 2811.
(2) (a) Cody, J. A.; Mansuetto, M. F.; Pell, M. A.; Chien, S.; Ibers, J. A. *J. Alloys Compd.* **1995**, *219*, 59. (b) Cody, J. A.; Ibers, J. A. *Inorg. Chem.* **1995**, *34*, 3165.
(3) Sutorik, A. C.; Albritton-Thomas, J.; Hogan, T.; Kannewurf, C. R.; Kanatzidis, M. G. *Chem. Mater.* **1996**, *8*, 751.
(4) Tougait, O.; Daoudi, A.; Potel, M.; Nöel, H. *Mater. Res. Bull.* **1997**, *32*, 1239.
(5) Chondroudis, K.; Kanatzidis, M. G. *C. R. Acad. Sci. Paris* **1996**, *322*, 887.
(6) Piccoli P. M. B.; Abney K. D.; Schoonover J. R.; Dorhout P. K. *Inorg. Chem.* **2000**, *39* (14), 2970−2976.
(7) Chondroudis, K.; Kanatzidis, M. G. *J. Am. Chem. Soc.* **1997**, *119*, 2574.
(8) Sutorik, A. C.; Patschke, R.; Schindler, J.; Kannewurf, C. R.; Kanatzidis, M. G. *Chem. Eur. J.* **2000**, *6*, 1601−1607.
(9) Choi, K.-S.; Kanatzidis, M. G. *Chem. Mater.* **1999**, *11* (9), 2613.
(10) Daoudi, A.; Lamire, M.; Levet, J. C.; Nöel, H. *J. Solid State Chem.* **1996**, *123*, 331.
(11) (a) Nöel, H.; Potel, M. *J. Less-Common Met.* **1985**, *113*, 11. (b) Nöel, H. *J. Less-Common Met.* **1980**, *72*, 45.
(12) Narducci, A. A.; Ibers, J. A. *Inorg. Chem.* **1998**, *37* (15), 3798.
(13) Sourisseau, C.; Gwet, S. P.; Gard, P. *J. Solid State Chem.* **1988**, *72*, 257 and references therein.
(14) Finckh, W.; Felser, C.; Tremel, W.; Ouvrard, G. *J. Alloys Compd.* **1997**, *262*, 97.
(15) (a) Cody, J. A.; Ibers, J. A. *Inorg. Chem.* **1996**, *35*, 3836. (b) Wu, E. J.; Pell, M. A.; Ibers, J. A. *J. Alloys. Comput.* **1997**, *255*, 106. (c) Choi, K.-S.; Patschke, R.; Billinge, S. J. L.; Waner, M. J.; Dantus, M.; Kanatzidis, M. G. *J. Am. Chem. Soc.* **1998**, *120*, 10706.

10.1021/ja0042534 CCC: $20.00
Published on Web 05/01/2001

the ThQ_3 $ZrSe_3$-type layers. In the case of ATh_2Se_6 electron diffraction experiments showed the Se atoms in the structure to adopt a long-range superstructure not detected by the X-ray single-crystal analysis. Here, we report on the structure and physicochemical properties of Cu_xUTe_3 ($x = 0.25$ and 0.33) that also present long-range superstructures, the details of which depend on the value of x. This is the result of local distortions that we discuss with respect to the parent binary phase, α-UTe_3. Furthermore, we present pair distribution function (PDF) data, based on the *total* X-ray scattering of Cu_xUTe_3 and α-UTe_3, to show that these two nearly isostructural phases, have substantially different local structure. This is much more so than what is suggested by the single-crystal X-ray analysis. We also present a convenient "chimie douche" route for the rational preparation of Cu_xUTe_3 from Cu and α-UTe_3.

Experimental Section

Reagents. The following reagents were used as obtained: (i) copper powder, 99.9% pure, Fisher Scientific Co., Fairlawn, NJ; (ii) uranium powder, 99.7% pure, 60 mesh, Cerac, Milwaukee, WI; and (iii) tellurium shots, 99.9% pure, Noranda Advanced Materials, Saint-Laurent, Quebec, Canada.

Synthesis of Cu_xUTe_3 ($x = 0.25$ and 0.33). Amounts of 0.076 g (3.0 mmol) of Cu, 0.095 g (1.0 mmol) of U, and 0.204 g (4.0 mmol) of Te were weighed into a vial in an N_2-filled glovebox. The starting materials were mixed thoroughly and loaded into a carbon-coated silica ampule. The ampule was then evacuated to $<1 \times 10^{-4}$ mbar and flame-sealed. In a computer-controlled furnace, the reaction was heated to 800 °C over 36 h, held at that temperature for 6 days, cooled to 400 °C at 4 °C/h, further cooled to 100 °C at 6 °C/h, and quenched to 50 °C. The ampule was opened in air to reveal the product, which consisted of purple cubes (25%), black powder (25%), and silver needles and plates (50%). All entities of the product are air and water stable. The purple cubes and black powder were identified by semiquantitative energy dispersive spectroscopy (EDS) to be Cu_2Te and UTe_3, respectively. The silver needles and plates gave the same average composition of $Cu_xU_{1.0}Te_{2.7-2.9}$ (x varied from 0.16 to 0.35).

Physical Measurements. (a) Powder X-ray Diffraction. Analyses were performed by using a calibrated Rigaku Rotoflex rotating anode powder diffractometer controlled by an IBM computer and operating at 45 kV/100 mA with a 1 deg K/min scan rate, employing Ni-filtered Cu radiation. Powder patterns were calculated with the Cerius2 software.[16]

(b) Semiquantitative Energy Dispersive Spectroscopy (EDS). The analyses were performed on a JEOL JSM-35C scanning electron microscope (SEM) equipped with a Tracor Northern energy dispersive spectroscopy (EDS) detector. Data were acquired on several crystals using an accelerating voltage of 25 kV and 40 s accumulation time.

(c) X-ray Crystallography. For reasons outlined in the results and discussion section, several crystals were examined crystallographically. **Crystal 1:** A single crystal with dimensions of $0.02 \times 0.05 \times 0.10$ mm was mounted on the tip of a glass fiber. Intensity data were collected at room temperature on a Rigaku AFC6S four-circle automated diffractometer (Mo Kα radiation). Space group $P2_1/m$. Unit cell parameters: $a = 6.0944(11)$ Å, $b = 4.2158(11)$ Å, $c = 10.3668(9)$ Å, $\beta = 98.874(10)$, $V = 263.16(9)$ Å^3, $Z = 2$. An empirical absorption correction based on ψ-scans was applied to all data during initial stages of refinement. The structure was solved by direct methods with the SHELXTL[17] package of crystallographic programs. Final $R1/wR2$ (defined in Table 1) 6.26/20.08%. **Crystals 2 and 3:** Single crystals with dimensions of $0.03 \times 0.05 \times 0.08$ mm for crystal 2 and $0.03 \times 0.04 \times 0.10$ mm for crystal #3 were mounted on the tip of a glass fiber. Intensity data were collected at 173.1 K for crystal 2 and room temperature for crystal 3 on a Siemens SMART Platform CCD diffractometer using graphite monochromatized Mo Kα radiation. The data were collected over a full sphere of reciprocal space for both crystals, up to 56° in 2θ. The individual frames were measured with an ω rotation of 0.3° and an acquisition time of 60 s for crystal 2 and 30 s for crystal 3. The SMART[18] software was used for the data acquisitions and SAINT[19] for the data extractions and reductions. The absorption corrections were performed using SADABS.[20] The structures were solved with direct methods using the SHELXTL package of crystallographic programs. The complete data collection parameters and details of the structure solutions and refinements are given in Table 1. The fractional atomic coordinates, isotropic and anisotropic temperature factors, bond distances, and bond angles for crystal 3 are given in Tables 2−4.

Table 1. Summary of the Crystallographic Data and Structural Analysis for Cu_xUTe_3 ($x = 0.25$ and 0.33)

	crystal 2	crystal 3
chemical formula	$Cu_{0.33}UTe_3$	$Cu_{0.25}UTe_3$
crystal habit, color	needle, silvery black	needle, silvery black
radiation	Mo Kα (0.71073 Å)	Mo Kα (0.71073 Å)
crystal size, mm	$0.03 \times 0.05 \times 0.08$	$0.03 \times 0.04 \times 0.10$
temperature, K	173	293
crystal system	monoclinic	monoclinic
space group	$P2_1/m$	$P2_1/m$
a, Å	6.0901(12)	6.0838(12)
b, Å	4.2083(8)	4.2140(8)
c, Å	10.335(2)	10.361(2)
β, deg	98.95(3)	98.83(3)
V, Å^3	261.66(9)	262.47(9)
Z	2	2
μ, mm^{-1}	48.529	48.063
index ranges	$0 \le h \le 7$	$-8 \le h \le 7$
	$-5 \le k \le 5$	$-5 \le k \le 5$
	$-13 \le l \le 13$	$-13 \le l \le 13$
$2\theta_{max}$, deg	56	56
total no. of data	1692	2521
no. of unique data	691	692
R(int)	0.045	0.044
no of. parameters	32	32
final $R1/wR2$,[a] %	5.04/11.80	4.13/10.42
Goof	1.047	1.190

[a] $R1 = \sum(|F_o| - |F_c|)/\sum|F_o| wR2 = \{\sum[w(F_o^2 - F_c^2)^2]/\sum[w(F_o^2)^2]\}^{1/2}$.

Table 2. Fractional Atomic Coordinates ($\times 10^4$), Equivalent Isotropic Displacement Parameters (Å$^2 \times 10^3$), and Occupancies for $Cu_{0.25}UTe_3$ (Crystal 3) with Estimated Standard Deviations in Parentheses

atom	x	y	z	U_{eq},[a] Å^2	occ
U	0.7914(1)	1/4	0.1629(1)	0.0009(1)	1
Te(1)	0.2659(2)	1/4	0.0599(1)	0.0009(1)	1
Te(2)	0.4007(2)	1/4	0.6620(1)	0.0014(1)	1
Te(3)	0.9114(2)	1/4	0.6685(1)	0.0016(1)	1
Cu	0.0930(15)	1/4	0.4656(7)	0.0019(2)	0.25

[a] U_{eq} is defined as one-third of the trace of the orthogonalized U_{ij} tensor.

Pair Distribution Function Analysis (PDF). The procedures used to perform atomic pair distribution function analysis of X-ray diffraction data have been published elsewhere.[21] The total scattering profiles of α-UTe_3 and $Cu_{0.3}UTe_3$ (nominal composition prepared by Cu insertion) were collected with use of the high-energy diffraction beamline (11ID-C) available in the BESSRC-CAT at the Advanced Photon Source located at Argonne National Laboratory. This beamline uses an elliptical multipole wiggler to provide extremely high energy X-rays (114.95 keV; $\lambda = 0.10786$ Å) at high flux. The high energy available at the

(16) *CERIUS*^{2}, Version 2.0; Molecular Simulations Inc.: Cambridge, England, 1995.

(17) Sheldrick, G. M. *SHELXTL*, Version 5; Siemens Analytical Xray Systems, Inc.: Madison, WI, 1994.

(18) *SMART*: Siemens Analytical Xray Systems, Inc.: Madison, WI, 1994.

(19) *SAINT*, Version 4.0; Siemens Analytical Xray Systems, Inc.: Madison WI, 1994−1996.

(20) *SADABS*; Sheldrick, G. M.; University of Göttengen: Göttengen, Germany, submitted for publication.

(21) (a) Egami, T. *Mater. Trans., JIM* **1990**, *31*, 163. (b) Billinge, S. J. L.; Egami, T. *Phys. Rev. B* **1993**, *47*, 14386. (c) Billinge, S. J. L.; DiFrancesco, R. G.; Kwei, G. H.; Neumeier, J. J.; Thompson, J. D. *Phys. Rev. Lett.* **1996**, *77*, 715.

Table 3. Anisotropic Displacement Parameters ($Å^2 \times 10^3$) for $Cu_{0.25}UTe_3$ (Crystal 3) with Estimated Standard Deviations in Parentheses[a]

	U_{11}	U_{22}	U_{33}	U_{12}	U_{13}	U_{23}
U	0.0008(1)	0.0005(1)	0.0013(1)	0	0.0001(1)	0
Te(1)	0.0007(1)	0.0009(1)	0.0011(1)	0	0.0001(1)	0
Te(2)	0.0016(1)	0.0011(1)	0.0017(1)	0	0.0007(1)	0
Te(3)	0.0019(1)	0.0011(1)	0.0018(1)	0	−0.0004(1)	0
Cu[b]	0.0034(5)	0.0013(4)	0.0012(3)	0	0.0010(4)	0

[a] The anisotropic displacement factor exponent takes the following form: $-2\pi^2[h^2a^2U_{11} + ... + 2hka^*b^*U_{12}]$. [b] Corresponding *x*, *y*, *z* and U_{ij} values for Cu in crystal 2: 0.092591, 1/4, 0.464639. U_{ij} values: 0.02700, 0.01529, 0.01646, 0.00000, 0.00464, 0.00000.

11ID-C allows the collection of high momentum elastic scattering data (up to $q \sim 45$ Å^{-1}, where $q = 4\pi \sin\theta/\lambda$), while also minimizing the necessity for absorption and multiple-scattering corrections. The finely ground samples were placed in thin wall 2 mm glassy capillary tubes and mounted in an aluminum sample stage. The sample stage was mounted inside a liquid He cryostat that was cooled to 5.6(1) K. The relatively weak inelastic Compton scattering and fluorescence intensity were discarded using a narrow energy window of an energy dispersive Ge detector to obtain the raw scattering intensity. The intensity of the incident beam was monitored with a ion-chamber current diode detector and the raw data corrected for fluctuation of the intensity of the incident beam. The data were also corrected for detector dead-time and polarization effects. No background correction or secondary Compton correction was necessary due to the strong scattering power of these heavy element containing samples. The corrected scattering profiles, $I(q)$, were converted to the normalized profiles, $S(q)$, and the atomic pair distribution functions calculated with the program RAD.

Transmission Electron Microscopy. Electron diffraction studies were carried out on a JEOL 100CX transmission electron microscope (TEM) using an electron beam generated by a CeB_6 filament and an acceleration voltage of 120 kV. After the samples were ground to a fine powder in acetone, the specimens were prepared by dipping a carbon-coated grid in the suspension. The samples showed no decomposition under the electron beam.

Charge Transport Measurements. DC electrical conductivity and thermopower studies were performed on single crystals of the compound. Conductivity measurements were performed in the usual four-probe geometry with 60- and 25-mm-diameter gold wires used for the current and voltage electrodes, respectively. Measurements of the sample cross-sectional area and voltage probe separation were made with a calibrated binocular microscope. Conductivity data were obtained with the computer-automated system described elsewhere.[22] Thermoelectric power measurements were made with using a slow ac technique[23] with 60 μm gold wires serving to support and conduct heat to the sample, as well as to measure the voltage across the sample resulting from the applied temperature gradient. In both measurements, the gold electrodes were held in place on the sample with a conductive gold paste.

Conductivity specimens were mounted on interchangeable sample holders, and the thermopower specimens were mounted on a fixed sample holder/differential heater. Mounted samples were placed under vacuum (10^{-3} Torr) and heated to room temperature for 2−4 h to cure the gold contacts. For a variable-temperature run, data (conductivity or thermopower) were acquired during both sample cooling and warming to check reversibility. The average temperature drift rate during an experiment was kept below 1 deg K/min. Several variable-temperature runs were carried out for each sample to ensure reproducibility and stability. At a given temperature, reproducibility was within ±5%.

Results and Discussion

Structure. Because in the early stages of this work Cu_xUTe_3 was confused with α-UTe_3 due to the almost identical unit cell parameters, several crystals from the same batch were solved to ascertain the presence of copper and to probe the variation in the value of *x*. As a result three crystals were solved and refined; two gave $x \sim 0.25$ and one gave $x \sim 0.33$. This suggests that *x* can vary substantially although the range was not determined. The observed crystal structure of Cu_xUTe_3 ($x = 0.25$ and 0.33) viewed down the *b*-axis is shown in Figure 1. The three-dimensional framework is built from layers very similar to those found in $ZrSe_3$, which are linked together by copper atoms. In α-UTe_3, which adopts the $ZrSe_3$ structure type, each U atom is coordinated to eight Te atoms in a bicapped trigonal prismatic environment. These trigonal prisms stack along the *b*-axis to form wedge-shaped columns by sharing triangular faces. Layers are then formed when neighboring columns share both their capping and apex monotellurides, see Figure 2A. Within these layers, there are ditelluride units that orient with their Te−Te bonds parallel to the *a*-axis. The Te−Te bond distances are 2.751(1) Å within the ditelluride units and 3.350(1) Å between them. In Cu_xUTe_3 ($x = 0.25$ and 0.33), however, the Te−Te distances (Te2−Te3 = 3.098(2) Å, Te3−Te2 = 2.987(2) Å) are almost equal, giving rise to infinite chains running along the [100] direction. As we will show later, these chains are an artifact of the crystal structure analysis which averages out long-range modulations that give rise to local distortions and a superstructure.

The copper atom is stabilized in a distorted tetrahedral geometry and sits on a mirror plane that generates a pair of crystallographically related sites. The distance between these two sites is 2.556(4) Å. Although it is tempting to conclude the copper atoms may not sit on both sites at the same time due to the partial occupancy on this site, this distance is reasonable for a Cu−Cu d^{10}−d^{10} interaction and cannot be ruled out according to the pair distribution analysis presented later.

The cell parameters of Cu_xUTe_3 ($x = 0.25$ and 0.33), compared to those of α-UTe_3, show only a slight expansion along the *c*-axis of 0.0548 Å and a slight increase in the cell volume of 0.27 Å^3. Consequently, there is essentially no shift in the positions of the peaks in the X-ray powder diffraction pattern. As a result, Cu_xUTe_3 ($x = 0.25$ and 0.33) cannot be readily distinguished from α-UTe_3 by casual comparison of the two patterns.

The structure of Cu_xUTe_3 ($x = 0.25$ and 0.33) is similar to that of $Tl_{0.56}UTe_3$[4] (Figure 3). It is therefore instructive to compare these two structures and understand the differences they pose. Both compounds are built from layers of α-UTe_3 with metal atoms inserted between them on partially occupied sites. The difference, however, lies in both the way that the UTe_3 layers stack with respect to one another and how the metal cations insert between these layers. In Cu_xUTe_3 ($x = 0.25$ and 0.33), the layers of UTe_3 stack in such a way that tetrahedral pockets are formed between the layers for the copper atoms to reside. In $Tl_{0.56}UTe_3$, the layers shift with respect to one another so that a larger, square prismatic pocket is formed for the much larger thallium atom to reside. This shift in the layers completely changes the symmetry of the compound. While Cu_xUTe_3 ($x = 0.25$ and 0.33) remains isostructural to the α-UTe_3 (monoclinic), $Tl_{0.56}UTe_3$ is orthorhombic.

α- vs β- UTe_3. After the crystals of Cu_xUTe_3 ($x = 0.25$ and 0.33) were discovered in the reaction mixture, efforts were made to synthesize the compound as a single phase through a rational synthetic route. Since reactions of direct element combination led to a mixture of Cu_xUTe_3 ($x = 0.25$ and 0.33) as well as both the α- and β-type[24] UTe_3, we decided to prepare α-UTe_3 as a starting material for further reaction with copper in a second step. The problem we encountered was that α-UTe_3 is less

(22) Lyding, J. W.; Marcy, H. O.; Marks, T. J.; Kannewurf, C. R. *IEEE Trans. Instrum. Meas.* **1988**, *37*, 76.
(23) Marcy, H. O.; Marks, T. J.; Kannewurf, C. R. *IEEE Trans. 1nstrum. Meas.* **1990**, *39*, 756.

Table 4. Selected Distances (Å) and Bond Angles (deg) for $Cu_{0.25}UTe_3$ (Crystal 3) with Standard Deviations in Parentheses

Bond Distances							
U−Te(1)	3.1053(1) × 2	U−Te(2)	3.121(1) × 2	Cu−Te(2)	2.545(4) × 3	Te(2)−Te(3)	2.988(2)
U−Te(1)	3.209(1)	U−Te(3)	3.130(1) × 2	Cu−Te(3)	2.522(9) × 2	Te(2)−Te(3)	3.097(2)
U−Te(1)	3.230(1)			Cu−Te(3)	2.521(9)		

Bond Angles				
Te(1)−U−Te(1)	85.47(3) × 1	76.01(3) × 2	76.14(3) × 2	141.75(4) × 1
Te(1)−U−Te(2)	151.72(3) × 2	87.89(3) × 2	75.58(3) × 2	128.73(2) × 2
Te(1)−U−Te(3)	149.46(4) × 2	86.98(3) × 2	130.24(3) × 2	73.45(3) × 2
Te(2)−U−Te(3)	57.10(3) × 2	84.66(4) × 2	111.45(3) × 2	
Te(2)−U−Te(3)	73.2(2) × 2	112.6(2) × 2		
Te(3)−U−Te(3)	119.4(2) × 2	113.3(3) × 1		

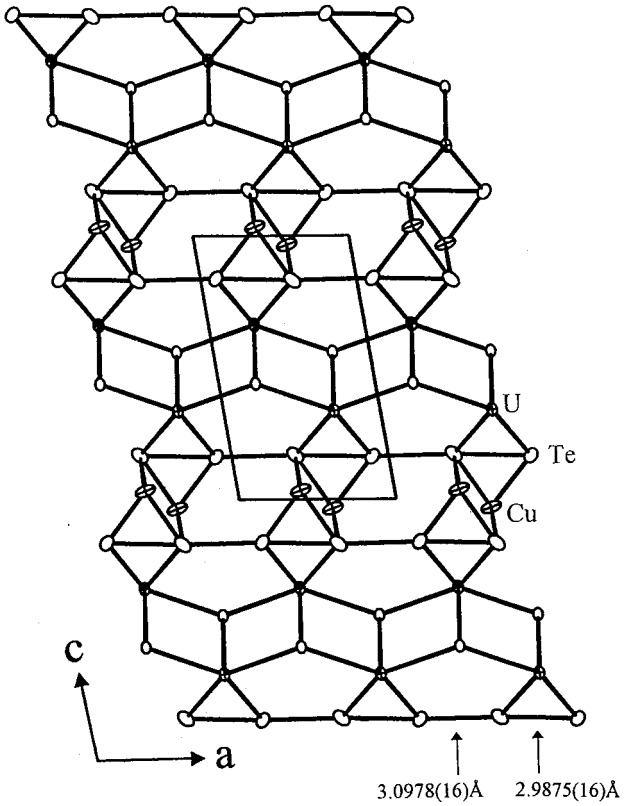

Figure 1. ORTEP representation of the structure of Cu_xUTe_3 (x = 0.25, 0.33) as seen down the *b*-axis (80% ellipsoids). The ellipses with octant shading represent U atoms. The crossed ellipses represent Cu atoms, and the open ellipses represent Te atoms.

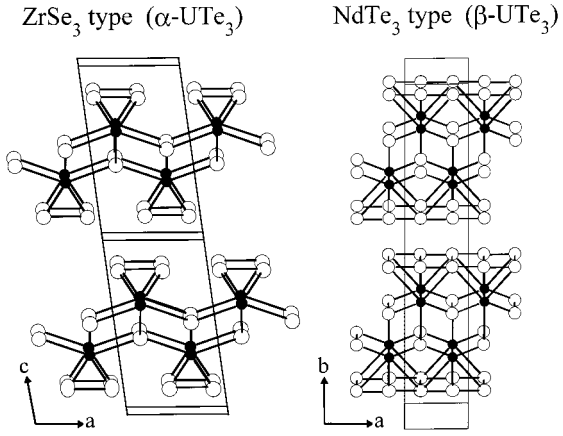

Figure 2. Extended stuctures of (A) α-UTe_3 and (B) β-UTe_3.

thermodynamically stable than β-UTe_3, making it difficult to prepare pure. The structural difference between the α- and β-UTe_3 lies in the coordination environment of the uranium

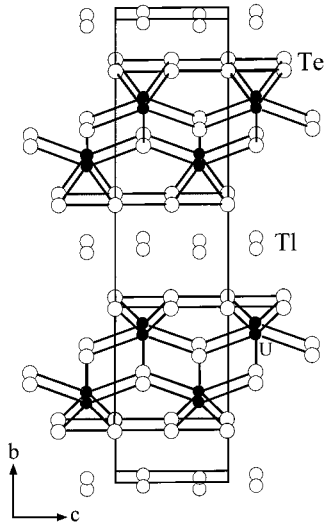

Figure 3. Extended structure of $Tl_{0.56}UTe_3$ as seen down the *b*-axis.

atoms. As previously described, α-UTe_3 (Figure 2A) consists of uranium atoms that are eight coordinate bicapped trigonal prismatic with rows of ditelluride atoms above and below the layers of uranium atoms. In β-UTe_3, which adopts the $NdTe_3$ structure type (see Figure 2B), the uranium atoms expand their coordination sphere to nine Te atoms in a tricapped trigonal prismatic arrangement. β-UTe_3 is structurally more dense and, as a result, the tellurium atoms above and below the plane of uranium atoms are best described as a square Te net. The literature reports the following synthesis for α-UTe_3.[25]

$$U + 3Te \xrightarrow[650\ ^\circ C]{1\ week} \text{grind} \xrightarrow[650\ ^\circ C]{1\ week} \alpha\text{-}UTe_3 \qquad (1)$$

Our attempts to reproduce this synthesis, however, resulted only in β-UTe_3. An added complication derived from the fact that there exist several other U_xTe_y binary compounds with similar compositions (i.e.: $UTe_{1.87}$,[26] UTe_2,[25,27] $UTe_{3.38}$,[25,26,28] $UTe_{3.4}$,[25,29] U_2Te_3,[30] UTe_5,[25,31] U_2Te_5,[25,32] U_3Te_5,[33] and U_7Te_{12}[34]). To avoid

(24) Nöel, H.; Levet, J. C. *J. Solid State Chem.* **1989**, *79*, 28.
(25) Boehme, D. R.; Nichols, M.; Snyder, R. L. *J. Alloys Compd.* **1992**, *179*, 37.
(26) Haneveld, A. J.; Klein, K.; Jellinek, F. *J. Less-Common Met.* **1969**, *18*, 123.
(27) (a) Stöwe, K. *J. Solid State Chem.* **1996**, *127*, 202. (b) Haneveld, A. J.; Klein, K.; Jellinek, F. *J. Less-Common Met.* **1970**, *21*, 45.
(28) Suski, W.; Wojakowski, A.; Blaise, A.; Salmon, P.; Fournier, J.; Mydlarz, T. *J. Magn. Mater.* **1976**, *3*, 195.
(29) (a) Breeze, E. W.; Brett, N. H. *J. Nucl. Mater.* **1971**, *40*, 113. (b) Breeze, E. W.; Brett, N. H.; White, J. *J. Nucl. Mater.* **1971**, *39*, 157.
(30) Tougait, O.; Potel, M.; Levet, J. C.; Nöel, H. *Eur. J. Solid State Inorg. Chem.* **1998**, *35*, 67.
(31) (a) Nöel, H. *Inorg. Chim. Acta* **1985**, *109*, 205. (b) Nöel, H. *Mater. Res. Bull.* **1984**, *19*, *1171*.
(32) (a) Tougait, O.; Potel, M.; Nöel, H. *J. Alloys Compd.* **1997**, *262*, 320. (b) Stöwe, K. *Z. Anorg. Allg. Chem.* **1996**, *622*, 1423.

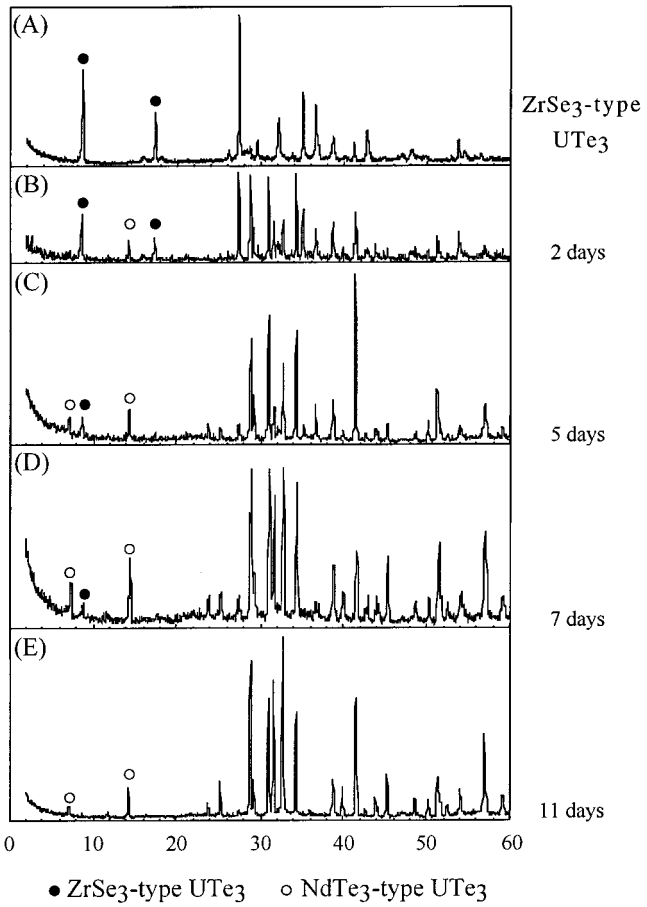

Figure 4. X-ray powder diffraction patterns of (A) α-UTe_3 and (B−E) the products of 1U + 3Te heated to 650 °C for 2, 5, 7, and 11 days.

these binary phases, a series of reactions were run with a U:Te ratio of 1:2.5 and the products were monitored as a function of time over the course of 5 days while heating at 525 °C. After 1 day, the product was determined by powder X-ray diffraction to be pure α-UTe_3. The powder patterns surprisingly did not change upon heating for up to 5 days and indicate that at a 1:2.5 ratio, α-UTe_3 will consistently form as a pure phase. In fact, it does not matter which temperature is chosen for this reaction to occur. As long as the ratio is 1:2.5, the mixture can be heated as high as 900 °C for 7 days to give α-UTe_3. When the ratio is changed to 1:3, however, the results were quite different. A second series of reactions were performed where U and Te were mixed in a ratio of 1:3 and heated to 650 °C from 1 to 11 days, see Figure 4. After 2 days, the product was a mixture of the α- and β-UTe_3. After 5−7 days, the product was still a mixture but the Bragg peaks corresponding to the β-UTe_3 grew in intensity while those corresponding to the α-UTe_3 decreased. After 11 days, the product consisted only of β-UTe_3. Finally, a set of experiments was conducted where the U to Te ratio was chosen to be 1:2.5, 1:3.0, 1:3.5, 1:4.0, and 1:4.5. The results, summarized in Table 5, show that at a U:Te ratio of 1:3 α-UTe_3 is less thermodynamically stable than β-UTe_3. The product formed depends more strongly on the amount of tellurium added rather than the temperature or time chosen for the reaction to occur. This raises the possibility that α-UTe_3 may in fact be a nonstoichiometric Te-deficient phase with considerable amount of U_2Te_5 possible as an intergrowth.

Table 5. Relative Stability of the UTe_3 Structure Types as a Function of the Amount of Tellurium Added[a]

reaction	product(s)
1U + 2.5Te	α-UTe3[b]
1U + 3.0Te	α- and β-UTe_3
1U + 3.5Te	α- and β-UTe_3
1U + 4.0Te	β-UTe_3
1U + 4.5Te	β-UTe_3

[a] The reaction was heated to 650 °C for one week. The products were determined by powder X-ray diffraction. [b] May contain slabs of the U_2Te_5 phase as an intergrowth.

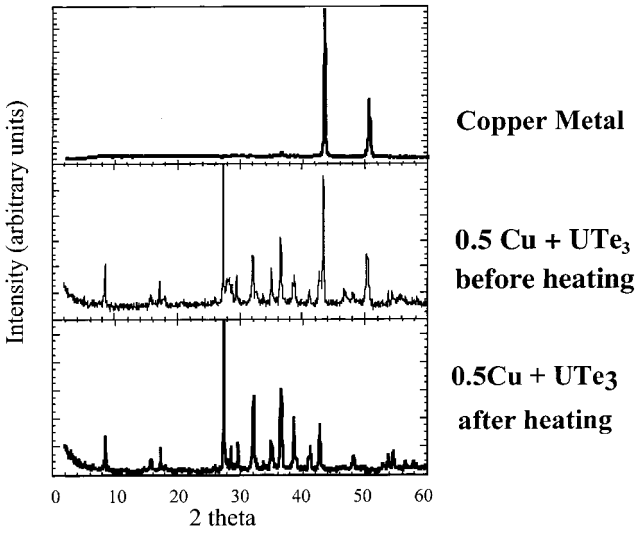

Figure 5. X-ray diffraction patterns of the Cu/α-UTe_3 system showing the "absorption" of Cu by the binary telluride to form Cu_xUTe_3.

Once the α-UTe_3 was prepared pure it was used as a starting material for further reactions with copper metal.

$$x\mathrm{Cu} + \alpha\text{-}UTe_3 \rightarrow Cu_xUTe_3 \qquad (2)$$

Mixtures of Cu and α-UTe_3 in the ratio of 0.25, 0.33, 0.5, 0.75, 1.0, 1.25, and 1.5 to 1.0 were pressed into pellets and heated at 300 °C for 2 days in a 13 mm Pyrex ampule that was flame sealed under vacuum.[35] The idea was that under mild heating conditions and close physical contact, the copper would be able to insert between the layers of UTe_3 and form the Cu_xUTe_3 ($x = 0.25$ and 0.33) phase. As discussed earlier, there is no recognizable difference in the positions of the peaks in the X-ray powder pattern of Cu_xUTe_3 ($x = 0.25$ and 0.33) and α-UTe_3. However, if the Bragg peaks corresponding to elemental copper decrease in intensity or even disappear, this could be indicative for copper insertion in α-UTe_3. The powder patterns of the elemental Cu, the reaction of 0.5Cu + 1.0α-UTe_3 before heating, and the product of 0.5Cu + 1.0α-UTe_3 after heating are shown in Figure 5. The peaks from elemental copper have noticeably disappeared, whereas the peaks due to UTe_3 are still there suggesting that Cu has successfully inserted between the layers to form the isostructural Cu_xUTe_3. The EDS analysis gives an average composition of $Cu_{0.35}UTe_3$, confirming that there is indeed Cu in the product.

The successful Cu insertion into the structure of UTe_3 via a relatively mild "chimie douche" route, using Cu metal, may in fact be a general synthetic method for the generation of a number or novel intercalative Cu derivatives of appropriate electron accepting host structures.

(33) Tougait, O.; Potel, M.; Nöel, H. *J. Solid State Chem.* **1998**, *139*, 356

(34) Tougait, O.; Potel, M.; Nöel, H. *Inorg. Chem.* **1998**, *37* (20), 5088.

(35) Note: The Cu metal was first activated by washing it with copious amounts of dilute hydrochloric acid. If this step is not taken, the oxide coating on the metal prevents it from reacting with the α-UTe_3.

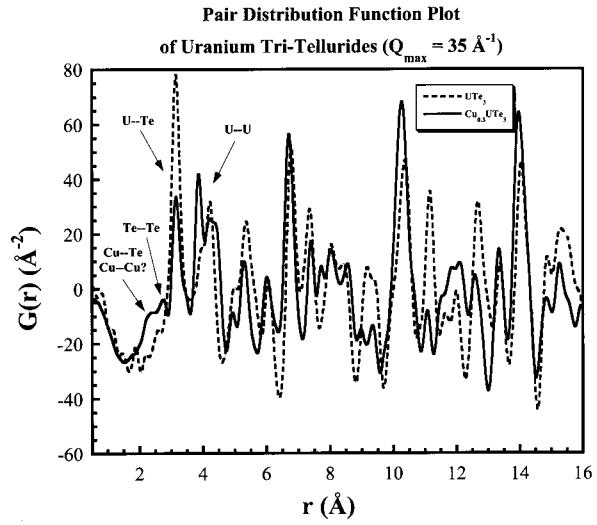

Figure 6. Atomic pair distribution function of α-UTe_3 and Cu_xUTe_3. The relevant interatomic vectors are shown.

Pair Distribution Function (PDF) Analysis. To prove whether the Cu had inserted between the layers, however, more direct evidence was needed. This was an important issue to resolve beyond any doubt if this type of reaction is to be proposed as a potential synthetic tool for Cu insertion chemistry. To solve this problem we used PDF analysis, a powerful experimental technique capable of probing the local structure of materials regardless of their degree of crystallinity. The PDF is very sensitive to the coordination environment of atoms over short (<5 Å) and intermediate (5−20 Å) ranges. The approach has proven to be quite successful in determining the structure of various materials exhibiting different degrees of structural disorder such as well-crystallized $La_{1-x}Ca_xMnO_{3.0}$[36−38] and disordered exfoliated-restacked WS_2.[39]

The PDF data obtained for α-UTe_3 and $Cu_{0.33}UTe_3$ are shown in Figure 6. The peaks at low interatomic distance **r** give us unique insight into the situation present in the first coordination sphere in both phases. In the copper intercalated phase, the peak at 2.75 Å is indicative of shortened Te−Te bonds, not present in the single crystal model. This argues strongly for significant local distortions, which may in fact be periodic as implied by the presence of a superstructure observed by electron diffraction (see below). The weak, broad shoulder at ∼2.5 Å is due to Cu−Te and possibly Cu−Cu vectors.[40] The observation of *both* a clear 2.5 Å shoulder *and* a 2.75 Å peak is strong evidence for the presence of Cu in the intercalated material.

The large peaks at 3.15 Å in both phases correspond to the first U−Te coordination shell. The breadth of these peaks reflects the range of U−Te vectors present. At slightly longer distances in the PDF of Cu_xUTe_3 we observe peaks around 3.9 and 4.2 Å which correspond to Te−Te and U−U vectors. In the parent α-UTe_3, the single-crystal model also indicates a single U−U distance of 4.22 Å, but the PDF of Cu_xUTe_3 clearly shows that the distribution of the 3.9 and 4.2 Å vectors is different, indicating a significant local distortion in the structure upon Cu insertion.

It is clear that the PDF data demonstrate the intercalation of copper into the α-UTe_3 structure, and the resulting compound has a distinct local structure, while at the larger distance regime, the overall structure appears qualitatively similar to the parent. Detailed modeling of the observed structural distortions needs to be performed to characterize these interesting local structures that are not observable in the Bragg data. Such work is currently in progress and the detailed structure analyses will be presented elsewhere.[41]

Superstructure. To balance the charges of Cu_xUTe_3 (x = 0.25 and 0.33), one must understand how the insertion of copper has affected the UTe_3 framework. To accommodate the extra +0.25 and +0.33 charge, some atoms in the framework must be reduced. Due to the close proximity of the so-called infinite Te chains to the copper atoms in the structure, it is most likely that these Te atoms act as the electron acceptors. This means that some of the Te−Te units in the parent α-UTe_3 structure will be reductively cleaved as indeed is observed crystallographically, see Figure 1 and Table 4. Therefore, a reasonable formula would be $(Cu^+)_x(U^{4+})(Te^{2-})(Te^{\left(\frac{1-x}{2}\right)})_2$. It is possible that such a reduction could cause a subtle superstructure to form whereby some of the Te−Te bonds in the chain are broken and some remain intact. Perhaps a clue for the presence of a superstructure comes from the anisotropic temperature factors, U_{11} and U_{33}, for the Te atoms in the chains (Te2 and Te3), which are larger than those of the uranium and Te1 atoms, see Table 3. Furthermore, the PDF data discussed above support the existence of normal Te−Te bonds (at ∼2.75 Å) in the structure which are "invisible" in the single-crystal structure analysis.

To probe such a superstructure, we used electron diffraction. Since it was not yet clear as to how the x-value of Cu_xUTe_3 (x = 0.25 and 0.33) would affect any potential modulation, the same crystals used for the X-ray structure determination (crystals 2 and 3) were carefully removed from the glass fiber and prepared for study by transmission electron microscopy (TEM). Diffraction was studied perpendicular to the UTe_3 layers. Both crystals showed evidence of a superstructure, see Figures 7 and 8. Remarkably, two different superstructures were found. When the amount of copper in the compound was 0.25, an incommensurate $6.25a_{sub} \times 1b_{sub}$ supercell was observed, while a commensurate supercell of $6a_{sub} \times 1b_{sub}$ was found when the amount of copper was 0.33. In contrast, corresponding electron diffraction experiments on α-UTe_3 show that there is no modulation in the structure. These results tell us that the amount of copper introduced between the layers directly affects how the Te chains in the structure distort by dictating how many Te_2^{2-} units are present. Therefore, based on the multifaceted experimental evidence presented above, we submit that the linear chains with almost equal Te−Te distances, observed by the single-crystal X-ray analysis, are an illusion caused by the averaging effect imposed from the substructure.

Charge Transport. Charge transport measurements were made on bulk crystals of Cu_xUTe_3 (x = 0.25 and 0.33) as well as on a polycrystalline pressed pellet of the binary α-UTe_3. The electrical conductivity and thermopower data on Cu_xUTe_3 (x = 0.25 and 0.33) are shown in Figure 9. The room-temperature conductivity reaches ∼280 S/cm and decreases with decreasing

(36) (a) Gutmann, M.; Billinge, S. J. L.; Brosha, E. L.; Kwei, G. H. *Phys. Rev. B* **2000**, *61*, 11762. (b) Proffen, Th.; DiFrancesco, R. G.; Billinge, S. J. L.; Brosha, E. L.; Kwei, G. H. *Phys. Rev. B* **1999**, *60*, 9973.

(37) Petkov, V.; DiFrancesco, R. G.; Billinge, S. J. L.; Acharaya, M.; Foley, H. C. *Phil. Mag.* **1999**, *B79*, 1519.

(38) (a) Toby, B. H.; Egami, T.; Jorgensen, J. D.; Subramanian, M. A. *Phys. Rev. Lett.* **1990**, *64* (20), 2414−2417. (b) Dmowksi, W.; Toby, B. H.; Egami, T.; Subramanian, M. A.; Gopalakrishnan, J.; Sleight, A. W. *Phys. Rev. Lett.* **1988**, *61* (22), 2608−2611.

(39) Petkov, V.; Billinge, S. J. L.; Heising, J.; Kanatzidis, M. G. *J. Am. Chem. Soc.* **2000**, *122*, 11571.

(40) The disordered single-crystal model suggests a pairing or chain formation of Cu atoms at 2.55 Å. Such a short Cu−Cu distance is reasonable considering that in Cu_2Te, the Cu−Cu distance at 2.45 Å is much shorter than the Cu−Te bond length of 2.67 Å (in Cu_2Te there are Te_2^{2-} units with a 2.82 Å bond length).

(41) Breshears J. D.; Kanatzidis M. G. Work in progress.

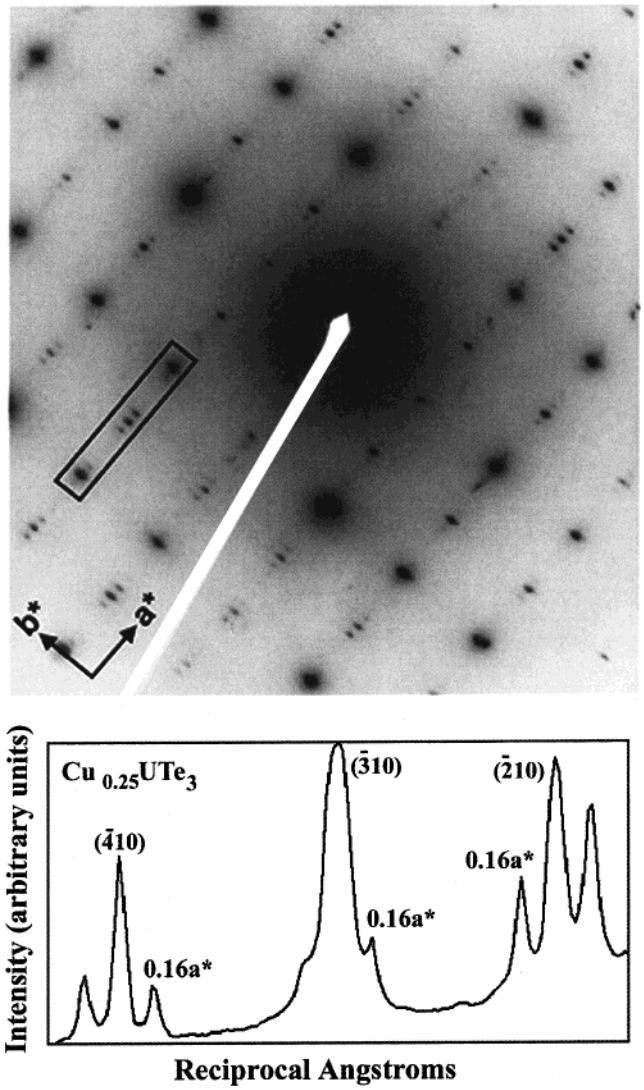

Figure 7. (A) Selected area electron diffraction pattern of $Cu_{0.25}UTe_3$ with the electron beam perpendicular to the layers ([001] direction) showing the incommensurate superlattice reflections along the *a**-axis. (B) Densitometric intensity scan along the *a**-axis of the electron diffraction pattern (boxed area on photograph) showing the (*h*10) family of reflections. The three reflections from the sublattice of $Cu_{0.25}UTe_3$ are indexed. The four weak peaks are from the superlattice with $a_{super} = 6.25a_{sub.}$

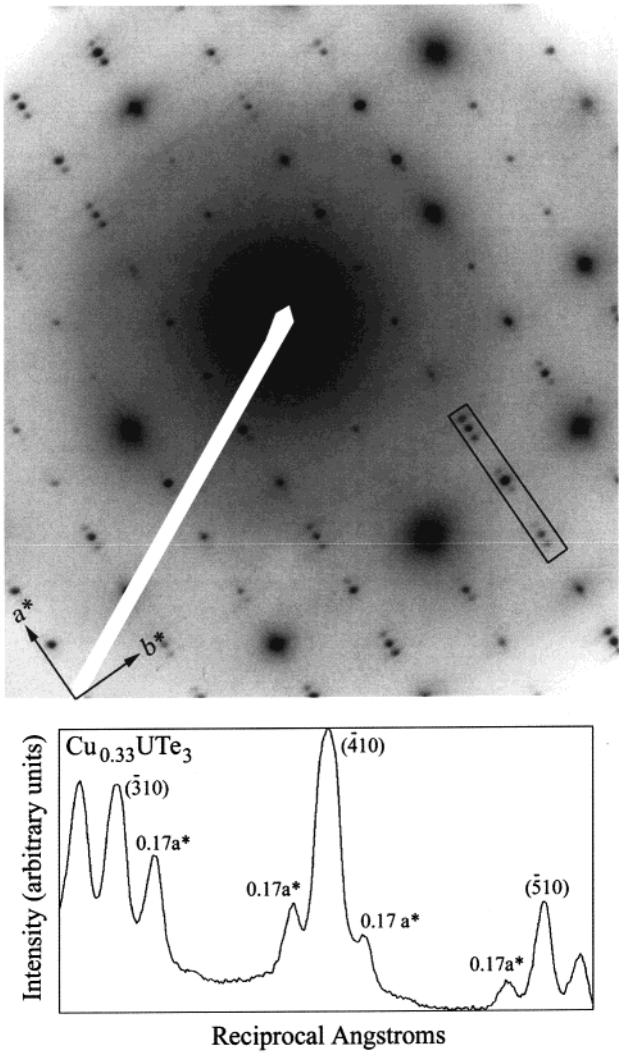

Figure 8. (A) Selected area electron diffraction pattern of $Cu_{0.33}UTe_3$ with the electron beam perpendicular to the layers ([001] direction) showing the commensurate superlattice reflections along the *a**-axis. (B) Densitometric intensity scan along the *a**-axis of the electron diffraction pattern (boxed area on photograph) showing the (*h*10) family of reflections. The three reflections from the sublattice of $Cu_{0.33}UTe_3$ are indexed. The four weak peaks are from the superlattice with $a_{super} = 6.0a_{sub.}$

temperature, suggesting a semiconductor. At 250 K there is an anomalous dip in the data. Interestingly, this dip also exists in the thermopower data at the same temperature. While we are unsure of the cause of this anomaly, we do not believe it is due to a structural transition since single-crystal X-ray data were collected for this compound both above and below this temperature and the same crystallographic structure was observed (see Table 1). The electrical conductivity of α-UTe_3 also indicates semiconducting behavior with a room-temperature value of 10 S/cm, almost 30 times less than Cu_xUTe_3 ($x = 0.25$ and 0.33). However, because these measurements were made on a pressed pellet this drop in conductivity might be largely due to grain boundary effects.

The thermopower data of Cu_xUTe_3 ($x = 0.25$ and 0.33) suggest that the material is a p-type semiconductor down to 40 K. Below this temperature, the material undergoes a p−n transition. At 300 K, the thermopower is 20 μV/K. In an attempt to further probe this transition from p-type to n-type, charge transport measurements were made on a pressed pellet of α-UTe_3, for comparison, see Figure 10. The thermopower data of α-UTe_3, which is insensitive to grain boundaries, give a behavior characteristic of a p-type narrow gap semiconductor with a room-temperature value of +550 μV/K. The data are lacking the p−n transition found in Cu_xUTe_3 ($x = 0.25$ and 0.33). From these measurements, it is evident that these properties are drastically affected by the insertion of copper between the layers of α-UTe_3. Due to the low temperature at which the p−n transition occurs for Cu_xUTe_3 it is difficult to ascertain the cause. We note, however, that a similar type of transition has been reported to occur in MTe_5 (M = Zr, Hf)[42] (at 80 K for $HfTe_5$ and 145 K for $ZrTe_5$) and to this date has defied explanation. Recently a theoretical treatment for these pentatellurides appeared in which the sign reversal of the thermopower and the resistivity anomalies were attributed to a two-component dielectric polaron conduction mechanism.[43]

(42) Littleton, R. T.; Tritt, T. M.; Feger, C. R.; Kolis, J. W.; Wilson, M. L.; Marone, M.; Payne, J.; Verebeli, D.; Levy, F. *Appl. Phys. Lett.* **1998**, *72* (16), 2056.

(43) Rubinstein, M. *J Appl. Phys.* **2000**, *87*, 5019−5021.

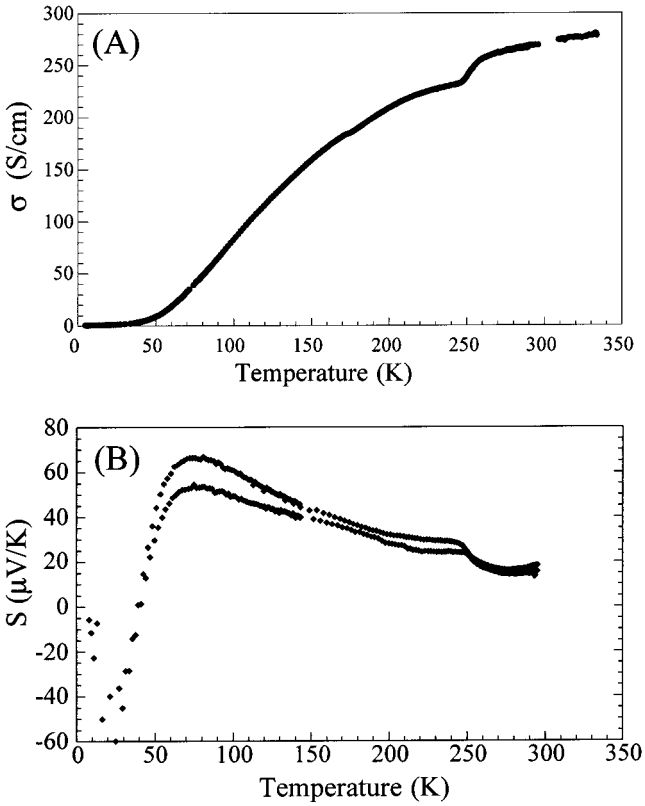

Figure 9. (A) Variable-temperature, four-probe electrical conductivity for a crystal of Cu_xUTe_3 ($x = 0.25$). (B) Variable-temperature thermopower data for a crystal of Cu_xUTe_3 ($x = 0.25$).

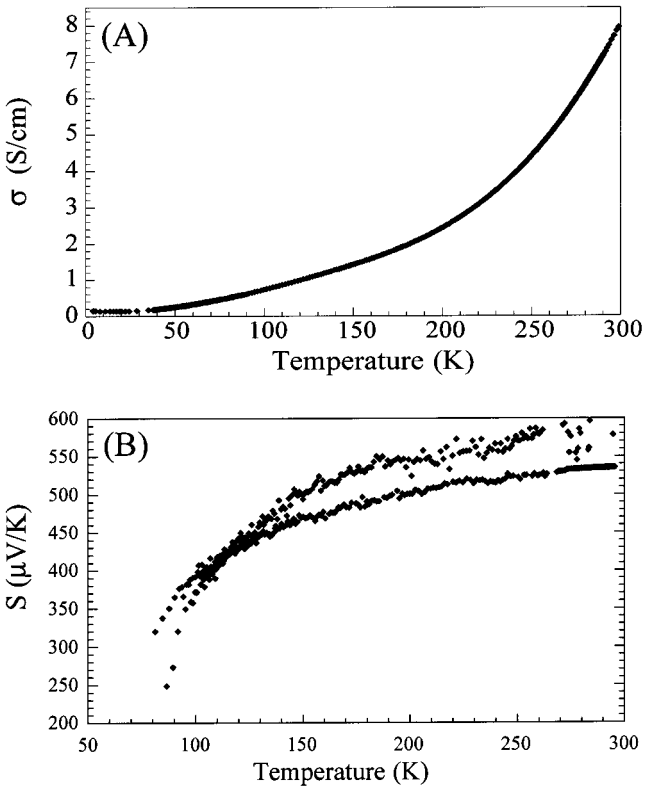

Figure 10. (A) Variable-temperature, four-probe electrical conductivity for a room-temperature pressed pellet of α-UTe_3. (B) Variable-temperature thermopower data for a room-temperature pressed pellet of α-UTe_3.

Conclusions

The discovery of Cu_xUTe_3 ($x = 0.25$ and 0.33) has provided us with the opportunity to take a closer look at the relative stabilities of the binary α,*β*-UTe_3 structure types. As a result we observe that α-UTe_3 is less thermodynamically stable than *β*-UTe_3 and that by using Te deficient conditions or by inserting Cu atoms between the layers of α-UTe_3 it is stabilized. Our attempts to insert Cu directly between the layers of α-UTe_3 through solid-state diffusion methods were successful and the convenient procedure we described may be a general "chimie douce" method for inserting Cu into suitable host materials of interest.[44]

PDF analysis not only demonstrates that Cu enters the structure but also indicates that the two supposedly isostructural phases, Cu_xUTe_3 and α-UTe_3, have substantially different local structures, much more so than what is suggested by the single-crystal X-ray analysis. This result demonstrates the utility of the analysis of *total* scattering data through the atomic pair distribution function method to obtain novel insights into the local coordination environment of extended solids. The PDF analysis has given us some insight as to how the structure of Cu_xUTe_3 ($x = 0.25$ and 0.33) may be stabilized. Finally, electron diffraction studies are critical in this case and indicate the existence a $6.0-6.25a_{sub} \times 1b_{sub}$ supercell. The type of supercell depends on the amount of copper in the compound and we believe it is electronically driven by structural modulations within the apparent Te−Te chains in the structure. These modulations are consistent with the local structure distortions observed by the PDF analysis. They involve the formation of normal Te−Te bonds at ∼2.75 Å and broken nonbonding Te−Te distances of >3.3 Å. Cu_xUTe_3 ($x = 0.25$ and 0.33) are semiconductors that present an interesting p−n transition at low temperatures as revealed by thermopower measurements. Further work on this fascinating material is in progress.

Acknowledgment. Financial support from the National Science Foundation (DMR-9817287) is gratefully acknowledged. This work made use of the SEM and TEM facilities of the Center for Advanced Microscopy at Michigan State University. We thank Dr. Valerie Petkov for help with the PDF data analysis and Drs. Lynn Soderholm, Uta Rütt, and S. Skanthakumar for help in obtaining PDF data at Argonne National Laboratory.

JA0042534

(44) (a) Others have reported on the electrochemical insertion of Cu in $ZrTe_3$. It would be interesting to see if Cu can be inserted in α-UTe_3 electrochemically. (b) Finchk, W.; Felser, C.; Tremel, W.; Ouvrard, G. *J. Alloys Compd.* **1997**, *97*, 262.